Applied Surface Science 314 (2014) 746–753

Contents lists available at ScienceDirect

Applied Surface Science

journal homepage: www.elsevier.com/locate/apsusc

Cobalt nanoparticles-embedded magnetic ordered mesoporous carbon for highly effective adsorption of rhodamine B

Lin Tang[a,b,*], Ye Cai[a,b], Guide Yang[a,b], Yuanyuan Liu[a,b], Guangming Zeng[a,b,*], Yaoyu Zhou[a,b], Sisi Li[a,b], Jiajia Wang[a,b], Sheng Zhang[a,b], Yan Fang[a,b], Yibin He[a,b]

[a] College of Environmental Science and Engineering, Hunan University, Changsha 410082, PR China
[b] Key Laboratory of Environmental Biology and Pollution Control, Hunan University, Ministry of Education, Changsha 410082, PR China

ARTICLE INFO

Article history:
Received 2 April 2014
Received in revised form 7 June 2014
Accepted 12 July 2014
Available online 19 July 2014

Keywords:
Cobalt nanoparticles-embedded magnetic ordered mesoporous carbon
Rhodamine B
Adsorption
Kinetics
Magnetic separation

ABSTRACT

Cobalt nanoparticles-embedded magnetic ordered mesoporous carbon (Co/OMC), prepared through a simple method involving infusing and calcination, was used as a highly effective adsorbent for rhodamine B (Rh B) removal. Several techniques, including SEM, HRTEM, nitrogen adsorption–desorption isotherms, XRD, Raman spectra, EDX, zeta potential and VSM measurement, were applied to characterize the adsorbent. Batch tests were conducted to investigate the adsorption performance. The adsorption capacity of the resultant adsorbent was relatively high compared with raw ordered mesoporous carbon (OMC) and reached an equilibrium value of 468 mg/g at 200 mg/L initial Rh B concentration. Removal efficiency even reached 96% within 25 min at 100 mg/L initial Rh B concentration. Besides, the adsorption amount increased with the increase of solution pH, adsorbent dose and initial Rh B concentration. Kinetics study showed that the adsorption agreed well with pseudo-second-order model (R^2 = 0.999) and had a significant correlation with intra-particle diffusion model in the both two adsorption periods. Furthermore, thermodynamics research indicated that the adsorption process was endothermic and spontaneous in nature. The adsorption isotherms fitted well with Langmuir model, demonstrating the formation of mono-molecular layer on the surface of Co/OMC during adsorption process. The results confirmed that Co/OMC has the potential superiority in removal of Rh B from aqueous solution.

1. Introduction

Aqueous dye pollution, commonly caused by the wastewater discharged from textile, leather and paper industries, has emerged as one of most serious pollution in water especially in developing countries, severely threatening the living of aquatic life and mankind [1]. Many dyes are highly toxic, carcinogenic, and stable from light and oxidation. Dyes not only make water colorful but also do harm for the survival of flora and fauna [2]. For example, dyes will deleteriously affect the photosynthetic aquatic life due to the reduction of light penetration [3]. Thus, finding an effective and suitable way to eliminate dye contamination from wastewater has become an urgent issue.

As a whole, numerous treating methods are investigated for the removal of dyes. Coagulation and flocculation are good for dye removal but difficult to dehydrate on account of sludge generating [3,4]. Chemical oxidation exhibits superb removal efficiency, but may results in the formation of harmful byproducts [5]. Biodegradation and microorganism adsorption have been developed rapidly in recent years. However, their long period and low efficiency remains tough problems [6–8]. Nowadays, increasing attention is paid to other burgeoning technologies like adsorption using novelly functionalized adsorbent [9].

Currently, adsorption has been proved to be a simple, effective and time-saving technology for removal of dyes [10], in which the key technology is to exploit selective and efficient adsorbents [11,12]. Conventional adsorbents, including silica gel [13], activated alumina [14] and zeolite molecular sieve [15,16], display low removal efficiency. Resins are widely used as adsorbents for dyes removal, but their surface areas are low and subsequent treatment and regeneration are difficult [17]. Ordered mesoporous carbon, on the other hand, possessing unique physical and chemical properties, such as high specific surface area, large pore volume, chemical interests and good mechanical stability, gradually shows enormous advantages in adsorption [18]. Furthermore, the impregnation of metals into ordered mesoporous carbon can intensify and expand the adsorption performance, which has gained a rapidly growing interest. Introducing some metal sources into ordered mesoporous

* Corresponding author. Tel.: +86 731 88822778; fax: +86 731 88823701.
E-mail addresses: tanglin@hnu.edu.cn (L. Tang), zgming@hnu.edu.cn (G. Zeng).

http://dx.doi.org/10.1016/j.apsusc.2014.07.060
0169-4332/

carbon, such as Fe, Ni, Mn and Co, will provide magnetism and also the possibility of creating specific binding sites whose binding force is conducive to adsorption [19]. Meanwhile, this also made it easy to be separated from aqueous solution by applying an external magnetic field instead of centrifugation or filtration [20]. Among these metal sources, magnetic susceptibility of Ni and Mn are modest, whereas Co has the improved magnetic properties. Furthermore, the strong stability of Co effectively prevents the leaching of Co ion into acidic solution compared with Fe. In previous studies, Co is selected as an appropriate metal source to synthesize Co/OMC, which has been proposed as carrier and anode material applied in the construction of sensors [21] and lithium-ion batteries [22]. However, the study on the application of Co/OMC as adsorbent is rarely reported, and still calls for novelly emerged assembly techniques for higher adsorption capacity and efficiency.

In this paper, Co/OMC has been synthesized by employing cobalt oxide to modify ordered mesoporous carbon through a simple method involving infusing and then calcination. Co nanoparticles were directly doped into the surface and pores of OMC. After comprehensive characterization of its physicochemical properties, Co/OMC was used as adsorbent to remove Rh B from aqueous solution which was often employed as a selected representative dye molecule. The relevant parameters, such as pH, adsorbent dose, contact time and initial Rh B concentration were optimized for the best adsorption performance of Co/OMC. Adsorption kinetics, thermodynamics and adsorption isotherm were used to expound the specific adsorption mechanism. The regeneration and reuse was also investigated to study the actual application of Co/OMC.

2. Material and methods

2.1. Material

Pluronic copolymer P123 (EO20PO70EO20, EO = ethylene oxide, PO = propylene oxide) was purchased from Sigma–Aldrich (USA). All reagents used in the experiment were of analytical reagent grade, and solutions were prepared with high-purity water (18.25 MΩ/cm) from a Millipore Milli-Q water purification system.

2.2. Preparation of OMC

The mesostructured SBA-15 silica template was firstly synthesized following conventional hydrothermal synthesis method as reported [23]. Ordered mesoporous carbon (OMC) was prepared by impregnation method with slight alternations [24]. The typical synthesis procedure is carried out as follows: 1 g of calcined SBA-15 was added to a solution containing 1.25 g of sucrose, 0.14 g of H_2SO_4 and 5 g of H_2O. The resultant mixture was heated in an oven at 100 °C for 6 h and then 160 °C for another 6 h. Then the sample was treated again at 100 °C and 160 °C using the same drying oven after the addition of 0.8 g of sucrose, 0.09 g of H_2SO_4 and 5 g of H_2O. The polymer composites were then heat-treated in nitrogen flow at 900 °C for 5 h with a heating rate of 5 °C/min. The silica template was removed using 10 wt% NaOH aqueous solutions at 90 °C for 1 h. OMC was obtained after washing with distilled water until the solution was neutral and drying at 60 °C.

2.3. Preparation of Co/OMC

0.6 g OMC was added into the mixture containing 0.25 g $Co(NO_3)_2{\cdot}6H_2O$ and 15 mL ethanol, then stirred for 1 h to make the Co completely impregnated in the surface of OMC and dried in vacuum oven at 60 °C. Subsequently, the above mixture was heat-treated in nitrogen flow at 500 °C for 4 h with a heating rate of 2 °C/min [22]. The Co/OMC was obtained and the detailed synthesis routes of Co/OMC were shown in Fig. 1.

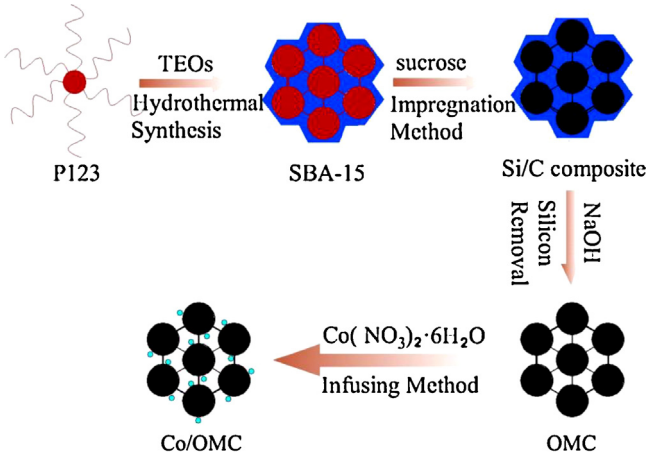

Fig. 1. Synthesis process of Co/OMC.

2.4. Characterization

High-resolution transmission electron microscopy (HRTEM) images were obtained on a JEOL-1230 electron microscope operated at 100 kV coupled with Energy-dispersive X-ray spectra (EDX) for elemental analysis of the material. Scanning electron microscope (SEM) images were recorded on a JEOL JSM-6700. Nitrogen adsorption–desorption isotherms were carried out on a Micromeritics 2020 analyzer at 77 K. The specific surface area and pore size distribution were calculated using the Brunauer–Emmett–Teller (BET) and Barrett–Joyner–Halenda (BJH) models respectively. XRD data were collected on a SIEMENSD 5005 diffractometer with Cu Ka, using a radiation at 40 kV and 30 mA. The zeta potentials of the materials were measured by Malvern ZEN3600 Zetasizer Nano. Raman spectroscopy was mounted using a LabRam HR800 Raman spectrometry.

2.5. Batch experiments

The adsorption of Rh B was performed by using batch technique in a thermostatic shaker bath at different Rh B initial concentrations, pH values, temperatures and adsorbent doses. In each set of experiment, 3 mg Co/OMC was added into 10 mL Rh B solution undergoing stirring at 25 °C for a certain time at 150 rpm. After adsorption, the supernatant was collected through magnetic separation for about 5 min and then the concentration of residual Rh B was measured using UV–vis spectrophotometer (UV-754N shanghai, China) at 554 nm. All experiments were performed in duplicate with the averaged values reported here. The removal efficiency (R, %), the amount of Rh B adsorbed at time t (q_t, mg/g) and at equilibrium (q_e, mg/g) were calculated using the following equations, respectively.

$$R = \frac{c_0 - c_t}{c_0} \times 100\% \quad (1)$$

$$q_t = \frac{(c_0 - c_t)V}{m} \quad (2)$$

$$q_e = \frac{(c_0 - c_e)V}{m} \quad (3)$$

where C_0, C_t and C_e (mg/L) were the initial, t time and equilibrium concentrations of Rh B solution, respectively; V (L) was the volume of Rh B solution and m (g) was the mass of Co/OMC.

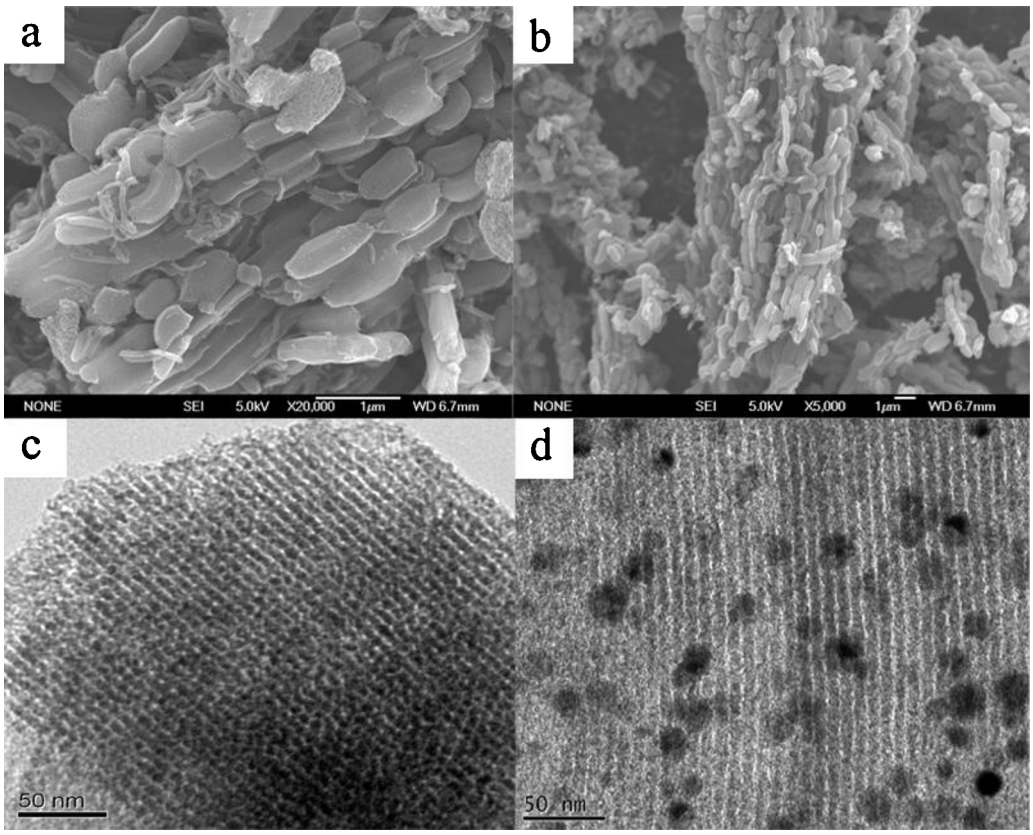

Fig. 2. SEM images of Co/OMC (a, b) and HRTEM images of OMC (c) and of Co/OMC (d).

For recycling tests, the regeneration of Co/OMC samples was achieved by using ethanol solution. Specifically, 3 mg of Co/OMC was first added into 10 mL of 100 mg/L Rh B solution for 3 h to reach adsorption equilibrium. Then, the used Co/OMC was extracted with an assistance of extra magnetic field before eluting with 10 mL of ethanol solution at 150 rpm for 12 h. Subsequently, the adsorbent was washed gently using pure water and then used in succeeding cycles.

3. Results and discussion

3.1. Characterizations of Co/OMC

Fig. 2 showed the scanning electron microscope (SEM) and high-resolution transmission electron microscopy (HRTEM) images of Co/OMC. From the SEM images in Fig. 2a and b, the rod-like morphology of Co/OMC period has been observed clearly, and the average length of each block was about 0.5 μm. The ordered mesopore structure of raw OMC and Co/OMC were clearly observed in the HRTEM image in Fig. 2c and d, indicating the modification scarcely has effect on the pore structure of ordered mesoporous materials. Magnetic Co nanoparticles with small particle size were uniformly dispersed in the carbon rods on the surface of OMC particles in Fig. 2d. The load of Co onto OMC surface had a little agglomeration, which slightly deteriorated the order of mesoporous but without affecting the skeleton structure of OMC. Fig. S1 and Table S1 presented the Energy-dispersive X-ray spectra (EDX) and the elemental analysis from EDX spectra of Co/OMC, respectively. As seen, the loading amount of Co was 8.92 wt%, which confirmed that Co nanoparticles had been successfully incorporated into the mesoporous material.

Nitrogen adsorption–desorption isotherms were recorded to investigate the surface and pore texture of the samples. Fig. 3 showed the results of nitrogen adsorption–desorption isotherms. The two isotherm curves both exhibited the representative type-IV curves with hysteresis loops, indicating the uniform mesoporous structure of raw OMC and Co/OMC. Table S2 showed the comparison of pore structure parameters of raw OMC and Co/OMC. The introduction of Co nanoparticles led to a distinct decrease in BET surface area (from 1237.8 to 955.3 m^2/g) and in pore volume (from 1.04 to 0.906 cm^3/g). Furthermore, the pore size of Co/OMC was 4.3 nm and showed a slight decrease compared with 4.71 nm of raw OMC, due to that the Co nanoparticles embedded blocked partial pores.

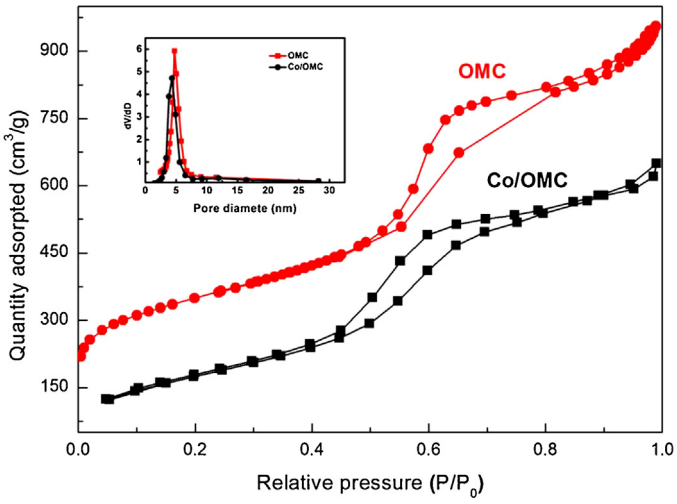

Fig. 3. Nitrogen adsorption–desorption isotherms and pore size distribution of OMC and Co/OMC.

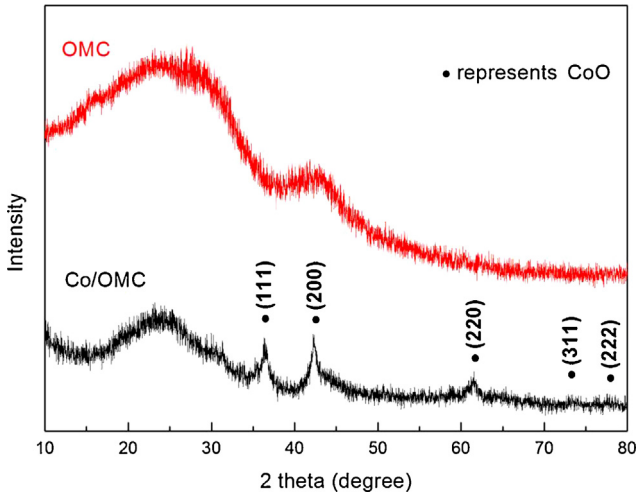

Fig. 4. XRD spectra of OMC and Co/OMC.

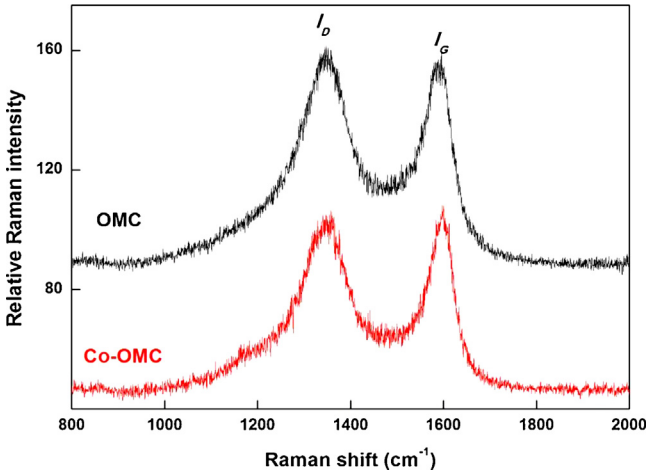

Fig. 5. Raman spectra of OMC and Co/OMC.

The wide-angle X-ray diffraction patterns of raw OMC and Co/OMC were shown in Fig. 4. It indicated that the two mesoporous materials exhibited broad peak at 24.8°, attributing to the graphitic carbon (0 0 2)-based plane diffraction. After the loading of Co nanoparticles, three well-resolved diffraction peaks appeared in the XRD pattern of Co/OMC emerging at 36.5°, 42.4°, 61.5°, which could be identified as the cubic structure of CoO for the planes of (1 1 1), (2 0 0), (2 2 0), respectively with the JCPDS card No.43-1004. The other two residual typical diffraction peaks of CoO at 73.7°, 77.5° corresponding to (2 1 1), (2 2 2) were relatively weak because of the low CoO loading amount among Co/OMC. Thus, the main form of Co existing in Co/OMC was CoO. Other cobalt oxides may also be developed through the synthesis process but could not be clearly seen in X-ray diffraction pattern probably due to the interference from the structure of OMC and low cobalt loading amount.

The Raman spectroscopy was usually conducted to reveal the structure of materials. The Raman spectra of raw OMC and Co/OMC composed of two characteristic peaks were represented in Fig. 5. The peak G near 1580 cm^{-1} was corresponding to the ordered structure of material surface, while the peak D near 1342 cm^{-1} represented the disordered structure. The ratio I_G/I_D unveiled the graphitization level of the pore wall structure. High level graphitization could enhance acid-base stability and oxidation resistance for the material. The ratio I_G/I_D of the materials increased after cobalt nanoparticles embedding compared with raw OMC,

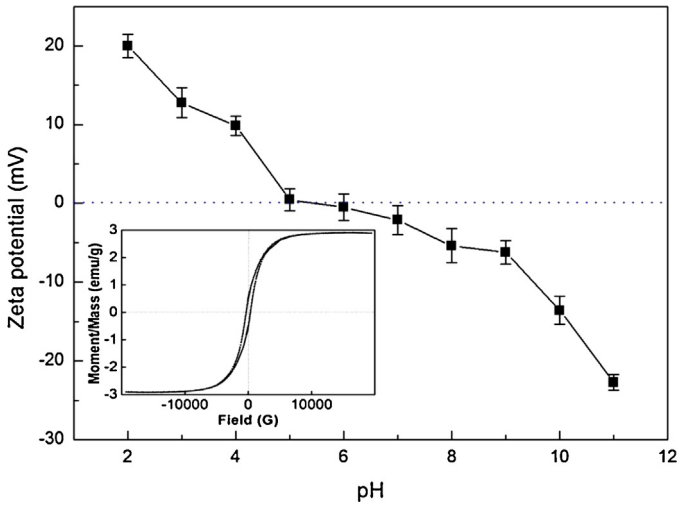

Fig. 6. Zeta potentials of Co/OMC at different solution pH. Inset is the Magnetization curves of Co/OMC.

indicating that the increase in graphitization of Co/OMC and the enhancement of material stability.

The VSM measurement was shown in the inset of Fig. 6. The saturation magnetization strength for Co/OMC was 2.9 emu/g, which was beneficial to separation. Hence, in the subsequent experiments, the separation of Co/OMC after finishing the adsorption was conducted by using magnet for about 5 min.

3.2. *Effect of initial pH*

The solution pH can significantly influence the surface charge and protonation of adsorbent which could be characterized by zeta potential shown in Fig. 6. The zero point of zeta potential was at 5.3. The surface of Co/OMC was positively charged when the solution pH was below 5.3, and became more and more negatively charged with the increasing of solution pH. When the pH varied from 2 to 5.3, there existed two factors affecting the adsorption, electrostatic repulsion and competitive force from H^+, which were both against Rh B removal, so the adsorption amount must be low. When the pH increased to 11, the electrostatic attraction turned to be favorable for adsorption and the competitive force gradually vanished. Hence, it would be more suitable for adsorption of Rh B onto Co/OMC at higher solution pH.

To study the influence of pH on the adsorption of Rh B, experiments at different pH were carried out at 25 °C for 3 h with 10 mL of 100 mg/L Rh B and 3 mg adsorbent. As shown in Fig. 7, we knew that the adsorption capacity reached the maximum at pH 9 for Co/OMC and pH 8 for OMC, which was in accordance with the results of zeta potential. The similar results have been reported by many studies on basic dye adsorption that adsorption capacity was low at strongly acidic solution, while increasing at higher pH values [25]. As pH increased from 2 to 7, the curve showed a sharp increase in adsorption capacity, which was mainly because of the recede of electrostatic repulsion and the decrease of competitive interactions from H^+. As pH increased from 7 to 9, the surface of material turned to be deprotonated, resulting in a strong binding force existing between the negatively charged adsorption sites and the cationic Rh B, which caused an increase in Rh B removal. Moreover, as compared to the OMC, Co/OMC exhibited higher adsorption capacity and broader optimal pH range, which showed its superiority over OMC in adsorption of Rh B. The solution pH was at their natural conditions in the following experiments in consideration of the little variation of adsorption amount from 321 mg/g to 323 mg/g with solution pH ranging from 7 to 9.

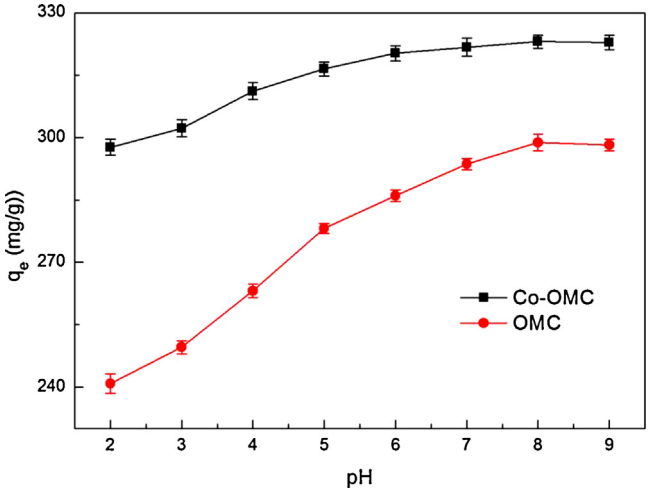

Fig. 7. Effect of pH values on adsorption of Rh B onto OMC and Co/OMC at 25 °C, within 3 h.

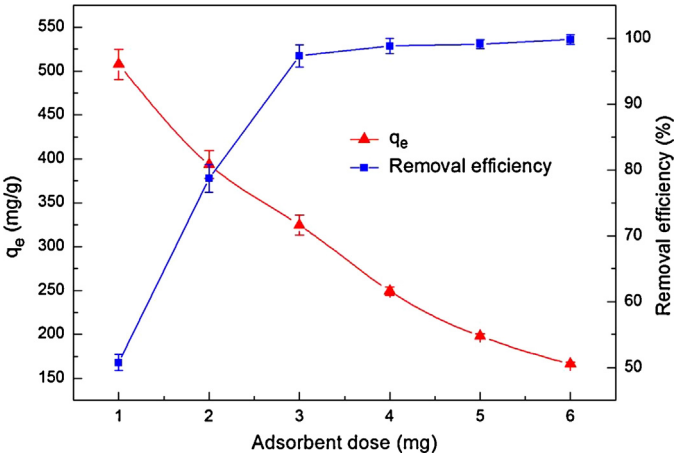

Fig. 8. Effect of adsorbent dose on adsorption of Rh B onto Co/OMC at 25 °C, within 3 h.

3.3. Effect of adsorbent dosage

Various amount of Co/OMC was added into 10 mL 100 mg/L Rh B aqueous solution at 25 °C for 3 h at 150 rpm. The results were shown in Fig. 8. It indicated that the removal efficiency increased from 50% to 99% with the increase of adsorbent dosage from 1 mg to 6 mg for more adsorption sites were available. Removal efficiency slightly increased with an increase in adsorbent dosage increase from 3 mg to 6 mg and subsequently reached equilibrium when Rh B molecular entirely occupied the available adsorption sites of Co/OMC. However, the adsorption capacity exhibited a gradual decrease from 507 mg/g to 166 mg/g with an increase in adsorbent amount. Therefore, adsorbent dose was maintained at 3 mg in the following experiments in consideration of both the high removal efficiency and adsorption amount.

3.4. Effect of contact time and initial concentration

Initial concentration was a significant factor that determines the adsorption amount and influences the equilibrium time of adsorption. The effect of contact time and initial concentration was presented in Fig. 9 with 3 mg Co/OMC at 25 °C at 150 rpm, where the initial Rh B concentration ranged from 50 mg/L to 200 mg/L, and contact time ranged from 0 to 240 minute. Results showed that adsorption equilibrium were both reached within 25 min at the

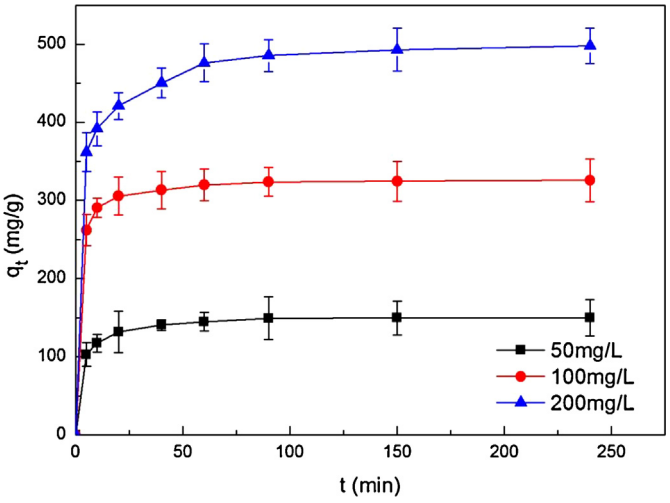

Fig. 9. Effect of contact time and initial concentration on adsorption of Rh B onto Co/OMC at 25 °C.

initial Rh B concentration of 50 mg/L and 100 mg/L, but within 60 min at 200 mg/L. At the first 25 min, the adsorption rate was very high due to the availability of abundant adsorption sites on the surface of Co/OMC, and the adsorption was observed less efficient after that for the saturation of these sites. It was indicated that adsorption rate was comparatively high for a strong binding force and affinity existing between adsorbent and adsorbate. The adsorption amount of Rh B was observed to increase immensely from 149 mg/g to 468 mg/g with initial Rh B concentration increased from 50 mg/L to 200 mg/L. High initial Rh B concentration expands the effective contact area with adsorbent and provides essential driving force to transcend the resistance to the mass transfer of Rh B on interface. Furthermore, the equilibrium adsorption amount and rate were relatively higher compared with previous researches on the removal of methylene green onto cobalt-embedded mesoporous carbon [26], which demonstrated that Co/OMC synthesized by this method had great superiority in dyes removal.

3.5. Adsorption kinetics

Adsorption kinetic model was applied to examine the rate of the adsorption process and to investigate the possible adsorption mechanisms of Rh B removal [27]. The pseudo-second-order model, one of the most widely used kinetic models, was adopted to investigate the adsorption process. The original pseudo-second-order equation was generally expressed as follows:

$$\frac{dq_t}{dt} = k(q_e - q_t)^2 \quad (4)$$

where q_e and q_t (mg/g) were the adsorption amounts of Rh B at equilibrium and at time t, respectively, and k (g/mg min) was the equilibrium rate constant of pseudo-second-order adsorption.

After the integration and variation by using boundary conditions of $t = 0$ to $t = t$, and $q = 0$ to $q = q_t$, the pseudo-second-order equation was given in linear as follows:

$$\frac{t}{q_t} = \frac{1}{kq_e^2} + \frac{t}{q_e} \quad (5)$$

The plot of t/q_t versus t was shown in Fig. 10. The parameters q_e and k could be calculated from the slope and intercept of the plot of t/q_t versus t and were given in Table 1. The values of correlation coefficient constant R^2 calculated from the linear fitting of pseudo-second-order equation were considerably high at all studied concentrations, which were all nearly 0.999.

Table 1
Adsorption kinetic model parameters for Rh B adsorption on Co/OMC at different Rh B initial concentrations.

Initial concentration (mg/L)	Pseudo-second-order			Intra-particle diffusion			
	k (g/mg min)	q_e (mg/g)	R^2	k_{i1} (mg/g min$^{1/2}$)	R_1^2	k_{i2} (mg/g min$^{1/2}$)	R_2^2
50	0.0025	151.7	0.9999	7.34	0.8876	0.51	0.8301
100	0.0023	327.9	0.9999	9.34	0.7808	0.6706	0.7101
200	0.0006	505.0	0.9998	20.01	0.9795	2.71	0.8976

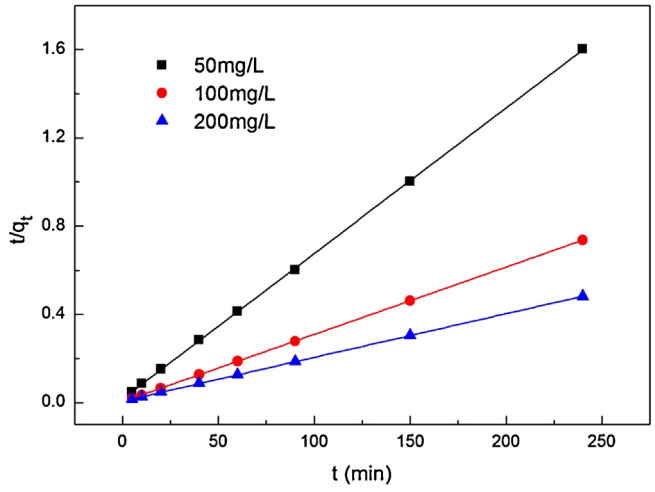

Fig. 10. Linear fit of experimental data using pseudo-second-order kinetic model.

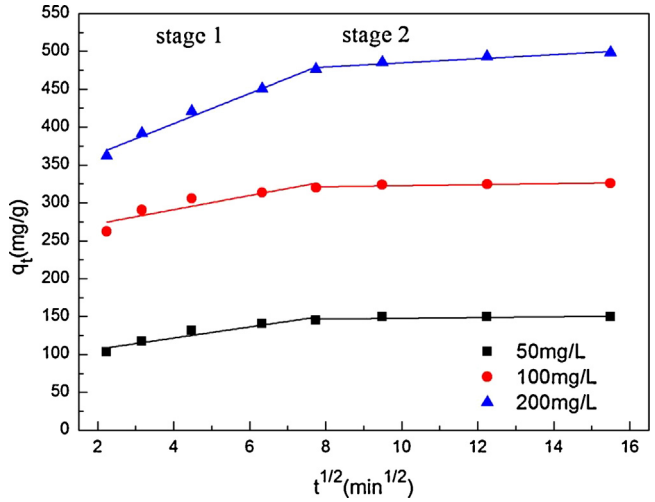

Fig. 11. Intra-particle diffusion model for Rh B adsorption onto Co/OMC.

Hence, the experiment data showed good accordance with pseudo-second-order model in terms of high correlation coefficient values, indicating that the rate-controlling step of chemisorptions was probably the valence forces produced by sharing or exchange of electrons between adsorbent and adsorbate. The same conclusion was also found in adsorption of Rh B by sodium montmorillonite [28] and activated carbon [29].

The intra-particle diffusion model proposed by Weber and Morris was also commonly used to characterize the sorption data, which was used to study the diffusion mechanism during the adsorption process. The plot of q_t versus $t^{1/2}$ was shown in Fig. 11. In general, if the plot of q_t versus $t^{1/2}$ gives a straight line and passes through the origin, the adsorption process is only controlled by the intra-particle diffusion model. If the plot of q_t versus $t^{1/2}$ gives a straight line but does not pass through the origin, the adsorption process is controlled partially by the intra-particle diffusion model.

Table 2
Thermodynamic parameters for Rh B adsorption on Co/OMC.

Temperature (°C)	ΔS (J/K mol)	ΔH (kJ/mol)	ΔG (kJ/mol)
25			−6.22
30			−7.31
35	218.08	58.77	−8.4
40			−9.5
50			−11.67

The intra-particle diffusion equation proposed could be written as follows:

$$q_t = k_i t^{1/2} + C \tag{6}$$

where k_i was the intra-particle diffusion rate constant (mg/g min), which could be calculated from the slope of the linear plot of q_t versus $t^{1/2}$, and C (mg/g) was the intercept.

As observed, the plot of q_t versus $t^{1/2}$ in Fig. 11 showed a double straight-line nature, suggesting that in the whole adsorption process intra-particle diffusion played a significant role but was not the only rate-controlling step. The value of k_i and R^2 were shown in Table 1. The data represented two periods of adsorption including the rapid adsorption (stage 1) and the stabilization (stage 2). The initially and rapid adsorption stage was probably attributed to the passage of Rh B molecule into the mesopores of Co/OMC which was corresponding to boundary layer diffusion. The second part was the residual adsorption process, indicating that the adsorption reached ultimate equilibrium. The same result could be found in adsorption of Rh B on activated carbon [29].

3.6. Adsorption thermodynamics

The Rh B adsorption process was conducted at different temperatures between 25 °C and 50 °C. The thermodynamic parameters such as free energy change (ΔG), enthalpy change (ΔH) and entropy change (ΔS) of adsorption were determined using the following equations:

$$\ln K_b = \frac{\Delta S}{R} - \frac{\Delta H}{RT} \tag{7}$$

$$\Delta G = \Delta H - T\,\Delta S \tag{8}$$

where c_e and q_e were the equilibrium concentration (mg/L) and the equilibrium adsorption amount (mg/g) of Rh B, respectively; R was the gas constant (J/mol K); T was the absolute temperature in Kelvin; ΔH (kJ/mol) and ΔS (kJ/mol) could be calculated from the slope and intercept of the linear plot of $\ln K_b$ versus $1/T$; and ΔG was calculated by Eq. (8).

The values of ΔH, ΔS and ΔG that obtained from the linear plots of $\ln K_b$ versus $1/T$, were summarized in Table 2. The ΔH of Rh B adsorption on Co/OMC was positive, indicating that the adsorption was an endothermic process in nature. The negative value of ΔG demonstrated the spontaneity and feasibility of the adsorption process of Rh B on the active sites of Co/OMC. Moreover, the positive value of ΔS confirmed the increased randomness at the solid–liquid interface during the adsorption of Rh B, in accordance with previous study [1].

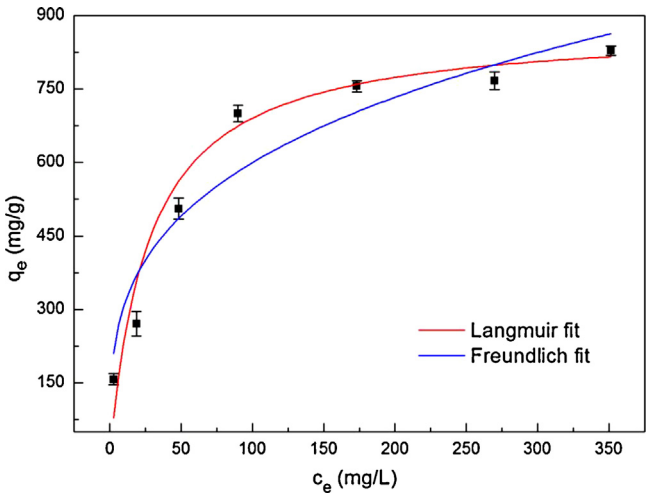

Fig. 12. Adsorption isotherms for Rh B removal onto Co/OMC using Langmuir and Freundlich isotherm model.

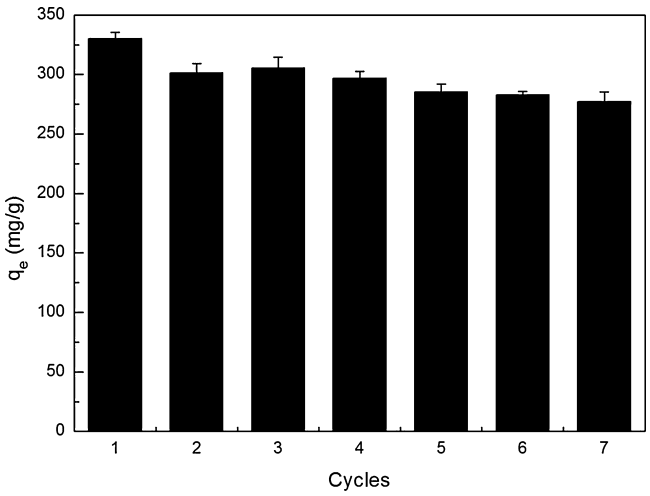

Fig. 13. Seven consecutive adsorption–desorption cycles of Co/OMC.

Table 3
Adsorption parameters for the Langmuir and Freundlich isotherm models.

Langmuir			Freundlich		
K_L (L/mg)	q_m (mg/g)	R_1^2	K_F	n	R_2^2
0.0366	879.45	0.9652	157.8	3.45	0.9401

3.7. Adsorption isotherms

In order to describe the adsorption process and investigate the mechanism of adsorption, two adsorption isotherm models namely Langmuir and Freundlich isotherms were applied to fit the experimental data. The Langmuir isotherm model [30] was based on the assumption that the adsorption process was a mono-molecular layer adsorption. The Freundlich isotherm [31] described adsorption onto a heterogeneous surface through a multilayer adsorption mechanism and the sites on the surface had different binding energies. The two models could be respectively expressed as follows:

$$\text{Langmuir}: \quad q_e = \frac{q_m K_L c_e}{1 + K_L c_e} \tag{9}$$

$$\text{Freundlich}: \quad q_e = K_F c_e^{1/n} \tag{10}$$

where q_e (mg/g) was the equilibrium amount of Rh B adsorption; q_m (mg/g) was the maximum adsorption capacity; c_e (mg/L) was the equilibrium solute concentration; K_L was the Langmuir constant representing the affinity of binding sites; and K_F and n were Freundlich constant and intensity factor, respectively.

The fitting results from the isotherms of the adsorption of Rh B on the Co/OMC were listed in Fig. 12. And the values of various parameters were also shown in Table 3. The results showed that Langmuir model can better describe the adsorption process for the higher correlation coefficient value ($R_1^2 = 0.9652$) compared with Freundlich model ($R_2^2 = 0.9401$), indicating the homogeneous adsorption of Rh B on Co/OMC. Meanwhile, it also revealed that the adsorbed Rh B formed a mono-molecular layer on the surface of Co/OMC and all sites on the surface needed the same energy during the binding process with Rh B.

The essential parameter of Langmuir adsorption isotherm could be represented in terms of a dimensionless constant called separation factor or equilibrium parameter (R_L), which was defined by the following Eq. (11):

$$R_L = \frac{1}{1 + K_L c_0} \tag{11}$$

where K_L (L/mg) was the Langmuir constant and C_0 (mg/L) was the Rh B concentration.

The R_L [32] value can indicate that the adsorption process is irreversible ($R_L = 0$), favorable ($0 < R_L < 1$), linear ($R_L = 1$) or unfavorable ($R_L > 1$). It was found that all values of R_L were positive. Thus, the adsorption of Rh B on Co/OMC was favorable and agreed well with Langmuir isotherm.

3.8. Regeneration of Co/OMC

To gain further insights into its actual application, the regeneration and reuse of Co/OMC was investigated using ethanol solution as eluent (Fig. 13). Fig. 13 showed the adsorption amount of Rh B over seven successive adsorption–desorption cycles. It was found that the adsorption capacity of Co/OMC was still high in the seventh regeneration cycle, with 277 mg/g of Rh B removal which is above 83% of the removal amount in first cycle, indicating that the resultant adsorbent could be regenerated and reused effectively by ethanol solution and allowed the treatment of wastewater contamination by Rh B in industry.

4. Conclusions

In this work, Co/OMC was successfully synthesized through a simple method involving impregnation and then calcination. The results showed that Co nanoparticles have been permeated in the surface and pore canals of OMC, and this material has the uniform mesoporous structure with weak magnetism. Batch experiment showed high effective and efficient removal capacity for Rh B. Adsorption equilibrium can be reached within 25 min to 60 min with equilibrium adsorption amount of 149 mg/g to 468 mg/g at initial concentration ranging from 50 mg/L to 200 mg/L. Equilibrium adsorption data was commendably fitted by pseudo-second-order kinetic model. The adsorption process was described well by the Langmuir model, indicating the homogeneous adsorption of Rh B on Co/OMC. The positive value of ΔH and the negative value of ΔG indicated the endothermic and spontaneous in nature of adsorption, respectively. The positive value of ΔS demonstrated that the randomness increase during the adsorption process. These results exhibited a compelling case that Co/OMC was an excellent adsorbent for dye removal with high adsorption capacity and efficiency, and can be easily separated using extra magnetic field before next use. With further development, Co/OMC might offer an effective treatment to remove dyes or even other simple organic pollutants from wastewater in industrial practice.

Acknowledgements

The study was financially supported by the Young Top-Notch Talent Support Program of China (2012), the National Natural Science Foundation of China (51222805), the Program for New Century Excellent Talents in University from the Ministry of Education of China (NCET-11-0129), Interdisciplinary Research Project of Hunan University, the Fundamental Research Funds for the Central Universities, Hunan University, and Foundation for the Author of Excellent Doctoral Dissertation of Hunan Province.

Appendix A. Supplementary data

Supplementary data associated with this article can be found, in the online version, at http://dx.doi.org/10.1016/j.apsusc.2014.07.060.

References

[1] P. Luo, Y.F. Zhao, B. Zhang, J.D. Liu, Y. Yang, J.F. Liu, Study on the adsorption of Neutral Red from aqueous solution onto halloysite nanotubes, Water Res. 44 (2010) 1489–1497.
[2] J. Anandkumar, B. Mandal, Adsorption of chromium(VI) and Rhodamine B by surface modified tannery waste: kinetic, mechanistic and thermodynamic studies, J. Hazard. Mater. 186 (2011) 1088–1096.
[3] K. Shakir, A.F. Elkafrawy, H.F. Ghoneimy, S.G.E. Beheir, M. Refaat, Removal of rhodamine B (a basic dye) and thoron (an acidic dye) from dilute aqueous solutions and wastewater simulants by ion flotation, Water Res. 44 (2010) 1449–1661.
[4] Z.F. Jiang, J.M. Xie, D.L. Jiang, Z.X. Yan, J.J. Jing, D. Liu, Enhanced adsorption of hydroxyl contained/anionic dyes on non functionalized Ni@SiO_2 core–shell nanoparticles: kinetic and thermodynamic profile, Appl. Surf. Sci. 292 (2014) 301–310.
[5] R. Jaina, M. Mathura, S. Sikarwara, A. Mittal, Removal of the hazardous dye rhodamine B through photocatalytic and adsorption treatments, J. Environ. Manage. 85 (2007) 956–964.
[6] T. Robinson, R. Marchant, P. Nigam, Remediation of dyes in textile effluent: a critical review on current treatment technologies with a proposed alternative, Bioresour. Technol. 77 (2001) 247–255.
[7] G. Crini, Non-conventional low-cost adsorbents for dye removal: a review, Bioresour. Technol. 97 (2006) 1061–1085.
[8] M. Constapel, M. Schellentrager, J.M. Marzinkowski, G. Siegmar, Degradation of reactive dyes in wastewater from the textile industry by ozone: analysis of the products by accurate mass, Water Res. 43 (2009) 733–743.
[9] S.A. Ahmed, E.M. Soliman, Silica coated magnetic particles using microwave synthesis for removal of dyes from natural water samples: synthesis, characterization, equilibrium, isotherm and kinetics studies, Appl. Surf. Sci. 284 (2013) 23–32.
[10] H.M.H. Gad, A.A. El-Sayed, Activated carbon from agricultural by-products for the removal of Rhodamine-B from aqueous solution, J. Hazard. Mater. 168 (2009) 1070–1081.
[11] X.M. Peng, X.J. Hu, D.F. Fu, F.L.Y. Lam, Adsorption removal of acid black 1 from aqueous solution using ordered mesoporous carbon, Appl. Surf. Sci. 294 (2014) 71–80.
[12] G.D. Yang, L. Tang, X.X. Lei, G.M. Zeng, Y. Cai, X. Wei, Y.Y. Zhou, S.S. Li, Y. Fang, Y. Zhang, Cd(II) removal from aqueous solution by adsorption on α-ketoglutaric acid-modified magnetic chitosan, Appl. Surf. Sci. 292 (2014) 710–716.
[13] S. Koner, A. Pal, A. Adak, Utilization of silica gel waste for adsorption of cationic surfactant and adsolubilization of organics from textile wastewater: a case study, Desalination 276 (2011) 142–147.
[14] T.K. Naiya, A.K. Bhattacharya, S.K. Das, Adsorption of Cd(II) and Pb(II) from aqueous solutions on activated alumina, J. Colloid Interface Sci. 333 (2009) 14–26.
[15] P. Aprea, D. Caputo, N. Gargiulo, F. Iucolano, F. Pepe, Modeling carbon dioxide adsorption on microporous substrates: comparison between Cu-BTC metal-organic framework and 13X zeolitic molecular sieve, J. Chem. Eng. Data 55 (2010) 3655–3661.
[16] R.X. Guo, J. Guo, F.Q. Yu, D.D. Gang, Synthesis and surface functional group modifications of ordered mesoporous carbons for resorcinol removal, Micropor. Mesopor. Mater. 175 (2013) 141–146.
[17] A. Vinu, K.Z. Hossian, P. Srinivasu, M. Miyahara, S. Anandan, N. Gokulakrishnan, Carboxy-mesoporous carbon and its excellent adsorption capability for proteins, J. Mater. Chem. 17 (2007) 1819–1825.
[18] Y.Y. Liu, Z.T. Zeng, G.M. Zeng, L. Tang, Y. Pang, Z. Li, C. Liu, X.X. Lei, M.S. Wu, P.Y. Ren, Z.F. Liu, M. Chen, G.X. Xie, Immobilization of laccase on magnetic bimodal mesoporous carbon and the application in the removal of phenolic compounds, Bioresour. Technol. 115 (2012) 21–26.
[19] T. Phenrat, Y.Q. Liu, R.D. Tilton, G.V. Lowry, Adsorbed polyelectrolyte coatings decrease Fe^0 nanoparticle reactivity with TCE in water: conceptual model and mechanisms, Environ. Sci. Technol. 43 (2009) 1507–1514.
[20] Y. Pang, G.M. Zeng, L. Tang, Y. Zhang, Y.Y. Liu, X.X. Lei, Z. Li, J.C. Zhang, G.X. Xie, PEI-grafted magnetic porous powder for highly effective adsorption of heavy metal ions, Desalination 281 (2011) 278–284.
[21] Y. Hou, J.C. Ndamanisha, L.P. Guo, X.J. Peng, J. Bai, Synthesis of ordered mesoporous carbon/cobalt oxide nanocomposite for determination of glutathione, Electrochim. Acta 54 (2009) 6166–6171.
[22] H.J. Zhang, H.H. Tao, Y. Jiang, Z. Jiao, M.H. Wu, B. Zhao, Ordered CoO/CMK-3 nanocomposites as the anode materials for lithium-ion batteries, J. Power Sources 195 (2010) 2950–2955.
[23] D. Zhao, Q. Huo, J. Feng, B.F. Chmelka, G.D. Stucky, Nonionic triblock and star diblock copolymer and oligomeric surfactant syntheses of highly ordered, hydrothermally stable, mesoporous silica structures, J. Am. Chem. Soc. 120 (1998) 6024–6036.
[24] S. Jun, S.H. Joo, R. Ryoo, M. Kruk, M. Jaroniec, Z. Liu, T. Ohsuna, O. Terasaki, Synthesis of new, nanoporous carbon with hexagonally ordered mesostructure, J. Am. Chem. Soc. 122 (2000) 10712–10713.
[25] M. Dogan, M. Alkan, Y. Onganer, Adsorption of methylene blue from aqueous solution onto perlite, Water Air Soil Pollut. 120 (2000) 229–248.
[26] M.Z. Dai, B.D. Vogt, High capacity magnetic mesoporous carbon-cobalt composite adsorbents for removal of methylene green from aqueous solutions, J. Colloid Interface Sci. 387 (2012) 127–134.
[27] L. Tang, G.D. Yang, G.M. Zeng, Y. Cai, S.S. Li, Y.Y. Zhou, Y. Pang, Y.Y. Liu, Y. Zhang, B. Luna, Synergistic effect of iron doped ordered mesoporous carbon on adsorption-coupled reduction of hexavalent chromium and the relative mechanism study, Chem. Eng. J. 239 (2014) 114–122.
[28] P.P. Selvam, S. Preethi, P. Basakaralingam, N. Thinakaran, A. Sivasamy, S. Sivanesan, Removal of rhodamine B from aqueous solution by adsorption onto sodium montmorillonite, J. Hazard. Mater. 155 (2008) 39–44.
[29] L. Li, S.X. Liu, T. Zhu, Application of activated carbon derived from scrap tires for adsorption of Rhodamine B, J. Environ. Sci. 22 (2010) 1273–1280.
[30] I. Langmuir, The adsorption of gases on plane surfaces of glass, mica and platinum, J. Am. Chem. Soc. 40 (1918) 1361–1403.
[31] H. Freundlich, Uber die adsorption in losungen, Z. Phys. Chem. 57 (1906) 385–470.
[32] K. Hall, L. Eagleton, A. Acrivos, T. Vermeulen, Pore- and solid-diffusion kinetics in fixed-bed adsorption under constant-pattern conditions, Ind. Eng. Chem. Fundam. 5 (1966) 212–223.